Mechanism of Rhodium-Catalyzed Intramolecular Hydroacylation: A Computational Study

I. F. Dempsey Hyatt, Heather K. Anderson, Andrew T. Morehead Jr.,* and Andrew L. Sargent*

Department of Chemistry, East Carolina University, Greenville, North Carolina 27858

Received August 21, 2007

All-electron numerical density functional theory calculations with scalar relativistic corrections have been utilized to examine the mechanism of the intramolecular rhodium-catalyzed hydroacylation reaction. The gas-phase results reveal a key branch point early in the reaction at the oxidative addition step wherein the two important pathways evolve through five-coordinate Rh(III) intermediates characterized by an apical acyl group and an equatorial hydride, orientations seemingly counter to trans influence arguments. These pathways account for the gross features of the experimental product distribution as well as the isotope labeling outcomes observed by previous investigators in this area. A greatly simplified approximation to modeling the reaction environment was applied that focused on redressing the coordinative unsaturation prevalent during certain steps of the catalytic process by including an explicit molecule of solvent or an additional molecule of substrate. Such an approach allowed us to explain the catalytic deactivation, substrate inhibition and dependence of the reaction rate on this coordinated ligand. Importantly, the application of a popular QM/MM method was unable to locate some of the key stationary points along the reaction path.

1. Introduction

The rhodium-catalyzed intramolecular hydroacylation reaction of 4-pentenals (eq 1) has been known for some time, and in 1988, Fairlie and Bosnich introduced what has become the standard method for carrying out the reaction.[1] Bosnich and co-workers also demonstrated the broad utility of chiral diphosphine rhodium complexes in the asymmetric cyclization of 4-pentenals.[2–6] In general, these reactions proceed in very high yields, with good turnover numbers (generally 50–300) and, when the appropriate chiral phosphine is utilized, with good to excellent enantioselectivities. Other investigators have also introduced many variants of this very useful reaction.[7–42]

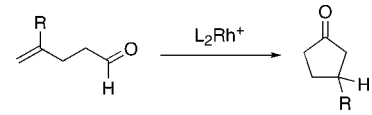

(1)

We have recently reported that the rhodium-catalyzed hydroacylation reaction of substituted 2-vinylbenzaldehyde results in an unusual dimerization reaction (eq 2) and that α-substituted

* To whom correspondence should be addressed. E-mail: moreheada@ecu.edu; sargenta@ecu.edu.

(1) Fairlie, D. P.; Bosnich, B. *Organometallics* **1988**, *7*, 936–945.
(2) Barnhart, R. W.; Bosnich, B. *Organometallics* **1995**, *14*, 4343–4348.
(3) Barnhart, R. W.; McMorran, D. A.; Bosnich, B. *Chem. Commun.* **1997**, 589–590.
(4) Barnhart, R. W.; McMorran, D. A.; Bosnich, B. *Inorg. Chim. Acta* **1997**, *263*, 1–7.
(5) Barnhart, R. W.; Wang, X.; Noheda, P.; Bergens, S. H.; Whelan, J.; Bosnich, B. *J. Am. Chem. Soc.* **1994**, *116*, 1821–1830.
(6) Bosnich, B. *Acc. Chem. Res.* **1998**, *31*, 667–674.
(7) Bendorf, H. D.; Colella, C. M.; Dixon, E. C.; Marchetti, M.; Matukonis, A. N.; Musselman, J. D.; Tiley, T. A. *Tetrahedron Lett.* **2002**, *43*, 7031–7034.
(8) Fu, G. C. In *Modern Rhodium-Catalyzed Organic Reactions*; Evans, P. A., Ed.; Wiley-VCH: New York, 2005; pp 79–91.
(9) Jun, C.-H.; Chung, J. H.; Lee, D.-Y.; Loupy, A.; Chatti, S. *Tetrahedron Lett.* **2001**, *42*, 4803–4805.
(10) Jun, C.-H.; Han, J.-S.; Yang, S.-S.; Chun, J. H. *Tetrahedron Lett.* **2001**, *42*, 4853–4856.
(11) Jun, C.-H.; Hong, J.-B.; Kim, Y.-H.; Chung, K.-Y. *Angew. Chem., Int. Ed.* **2000**, *39*, 3440–3442.
(12) Jun, C.-H.; Hong, J.-B.; Lee, D.-Y. *Synlett* **1999**, 1–12.
(13) Jun, C.-H.; Lee, D.-Y.; Lee, H.; Hong, J.-B. *Angew. Chem., Int. Ed.* **2000**, *39*, 3070–3072.
(14) Jun, C.-H.; Lee, H.; Hong, J.-B. *J. Org. Chem.* **1997**, *62*, 1200–1201.
(15) Jun, C.-H.; Lee, H.; Hong, J.-B.; Kwon, B.-I. *Angew. Chem., Int. Ed.* **2002**, *41*, 2146–2147.
(16) Jun, C.-H.; Lee, H.; Lin, S.-G. *J. Am. Chem. Soc.* **2001**, *123*, 751–752.
(17) Jun, C.-H.; Lee, J. H. *Pure Appl. Chem.* **2004**, *76*, 577–587.
(18) Jun, C.-H.; Lim, Y.-G. *Tetrahedron Lett.* **1995**, *36*, 3357–3360.
(19) Jun, C.-H.; Moon, C. W.; Lee, D.-Y. *Chem.−Eur. J.* **2002**, *8*, 2422–2428.
(20) Jun, C.-H.; Moon, C. W.; Lee, H.; Lee, D.-Y. *J. Mol. Cat. A: Chem.* **2002**, *189*, 145–156.
(21) Jun, C.-H.; Moon, C. W.; Lim, S.-G.; Lee, H. *Org. Lett.* **2002**, *4*, 1595–1597.
(22) Lenges, C. P.; Brookhart, M. *J. Am. Chem. Soc.* **1997**, *119*, 3165–3166.
(23) Lenges, C. P.; White, P. S.; Brookhart, M. *J. Am. Chem. Soc.* **1998**, *120*, 6965–6979.
(24) Lenges, C. P.; White, P. S.; Marshall, W. J.; Brookhart, M. *Organometallics* **2000**, *19*, 1247–1254.
(25) Moxham, G. L.; Randell-Sly, H. E.; Brayshaw, S. K.; Woodward, R. L.; Weller, A. S.; Willis, M. C. *Angew. Chem., Int. Ed.* **2006**, *45*, 7618–7622.
(26) Tanaka, K.; Fu, G. C. *J. Am. Chem. Soc.* **2001**, *123*, 11492–11493.
(27) Tanaka, K.; Fu, G. C. *Angew. Chem., Int. Ed.* **2002**, *41*, 1607–1609.
(28) Tanaka, K.; Tanaka, M.; Suemune, H. *Tetrahedron Lett.* **2005**, *46*, 6053–6056.
(29) Tanaka, M.; Imai, M.; Fujio, M.; Sakamoto, E.; Takahashi, M.; Eto-Kato, Y.; Wu, X. M.; Funakoshi, K.; Sakai, K.; Suemune, H. *J. Org. Chem.* **2000**, *65*, 5806–5816.
(30) Tanaka, M.; Imai, M.; Yamamoto, Y.; Tanaka, K.; Shimowatari, M.; Nagumo, S.; Kawahara, N.; Suemune, H. *Org. Lett.* **2003**, *5*, 1365–1367.
(31) Tanaka, M.; Sakai, K.; Suemune, H. *Curr. Org. Chem.* **2003**, *7*, 353–367.

10.1021/om700842d CCC: $40.75
Publication on Web 12/08/2007

2-vinylbenzaldehydes may be cyclized with chiral rhodium catalysts to give 3-substituted indanones in high yields and generally excellent enantioselectivities.[43] However, electron-rich substituents on the vinyl group result in lowered enantioselectivities and unusual kinetics that led us to consider a computational examination of the associated mechanism. In order to do so, we decided first to return to the well-understood system of Fairlie and Bosnich,[44] where abundant and detailed data already exist, to conduct a computational examination of the reaction mechanism for this prototype of intramolecular hydroacylation. The use of computational methods in elucidating organometallic reactions mechanisms is well established, and has been recently reviewed.[45–49] One previous computational study on hydroacylation has been reported,[50] and we will discuss those findings in greater depth below.

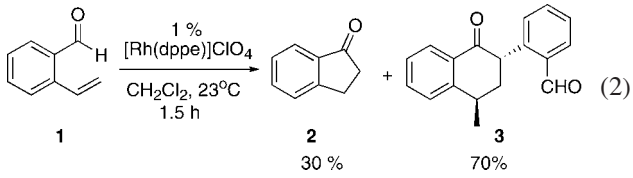

(2)

The basic catalytic cycle of hydroacylation, adapted from Fairlie and Bosnich, is shown in Scheme 1.[44] A rapid pre-equilibrium involving catalyst, solvent, and substrate is followed by intramolecular oxidative addition to form **7**, insertion to form **8** or **10**, and finally, an irreversible (under the reaction conditions) reductive elimination.

This basic mechanism was proposed by Bosnich following extensive deuterium-labeling studies, which revealed that the label was scrambled throughout the starting material to give labeling at both the 2- and 3-position of the resulting cyclopentanone.[44] The comprehensive mechanism shown in Scheme 2 gives a reasonable pathway to all products observed. Importantly, Bosnich postulated that reductive elimination must be the slow step to allow rapid pre-equilibria and interconversion of the intermediates shown in Scheme 2. Scrambled pentenals **4″**, **4‴**, and **4⁗** were all formed more rapidly than product **9′**, but competitively with **9**, demonstrating the rapid interconversion between the intermediates.

Scheme 1. Catalytic Cycle of Rhodium-Catalyzed Hydroacylation

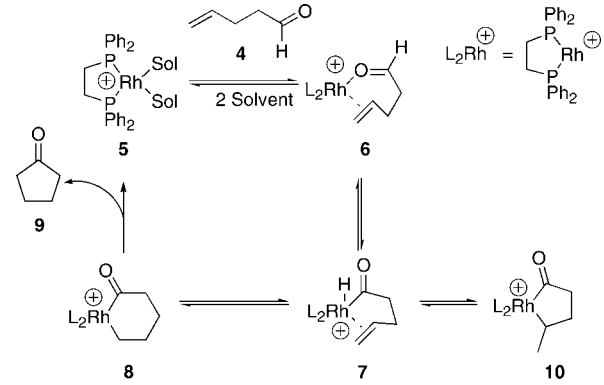

The major pathway leading to catalyst deactivation is decarbonylation of the aldehyde by the metal complex, postulated by Bosnich to proceed as shown in Scheme 3. He observed the generation of both 1- and 2-butenes (**16**) during the reaction and established that the monocarbonyl complex **15** can rapidly decarbonylate aldehydes to generate a catalytically inactive dicarbonyl complex **17**. It is important to note that these pathways must be minor, since turnover numbers greater than 100 are obtained in most cases. Bosnich postulated that the most likely pathway leading to decarbonylation was **7** → **12** → **15** + **16** due to the difficulty of β-hydride elimination from **11** or **13** but could not exclude these other two pathways based on their data.

Since many of the intermediates possess open coordination sites, it is expected that such sites will be filled with solvent or other coordinating species during the catalytic cycle. Fairlie and Bosnich found that dichloromethane and nitromethane were useful solvents for this reaction, while acetonitrile shut down catalysis, presumably by coordinating too strongly to the disolvento complex **5** (Scheme 1). Interestingly, they also observed that acetone gave approximately 20 rapid turnovers, followed by catalyst decarbonylation.

As might be expected from the multitude of pathways shown in Schemes 1–3, the kinetics of this system were found to be complex. In addition, none of the intermediates could be observed, meaning that the equilibria must be rapid and favor starting material and product. Interestingly, Bosnich found that substrate (**4**) acts to retard the rate of reaction via substrate inhibition while extending the lifetime of the catalyst (i.e., higher concentrations of **4** slow the reaction, but give higher turnover numbers). He postulated that coordination of the substrate to open coordination sites in species like **7** blocked the decarbonylation pathway. Substrate inhibition was attributed to the multiple pre-equilibria involving **4** and **5** that do not lead to the catalytically viable **6** (i.e., two substrate molecules (**4**) bound via the aldehyde).

As previously noted, none of the intermediates proposed by Bosnich in the catalytic cycle were spectroscopically observed or otherwise verified by direct methods. However, the wealth of data generated in his thorough experimental study set the stage for a follow-up computational analysis. It is in this context that we make the present report. Our goal is to derive an understanding of the fundamental mechanism of intramolecular catalytic hydroacylation and apply it to related catalytic vinylbenzaldehyde cyclizations in the near future.

The results are organized into the following sections. After an explanation of the computational methods, results corre-

(32) Tanaka, M.; Takahashi, M.; Sakamoto, E.; Imai, M.; Matsui, A.; Fujio, M.; Funakoshi, K.; Sakai, K.; Suemune, H. *Tetrahedron* **2001**, *57*, 1197–2004.
(33) Willis, M. C.; McNally, S. J.; Beswick, P. J. *Angew. Chem., Int. Ed.* **2004**, *43*, 340–343.
(34) Willis, M. C.; Randell-Sly, H. E.; Woodward, R. L.; Currie, G. S. *Org. Lett.* **2005**, *7*, 2249–2251.
(35) Willis, M. C.; Randell-Sly, H. E.; Woodward, R. L.; McNally, S. J.; Currie, G. S. *J. Org. Chem.* **2006**, *71*, 5291–5297.
(36) Willis, M. C.; Sapmaz, S. *Chem. Commun.* **2001**, 2558–2559.
(37) Marder, T. B.; Roe, D. C.; Milstein, D. *Organometallics* **1988**, *7*, 1451–1453.
(38) Milstein, D. *J. Chem. Soc., Chem. Commun.* **1982**, 1357–1358.
(39) Sakai, K.; Ide, J.; Oda, O.; Nakamura, N. *Tetrahedron Lett.* **1972**, 1287–1290.
(40) Suggs, J. W. *J. Am. Chem. Soc.* **1978**, *100*, 640–641.
(41) Roy, A. H.; Lenges, C. P.; Brookhart, M. *J. Am. Chem. Soc.* **2007**, *129*, 2082–2093.
(42) Taura, Y.; Tanaka, M.; Wu, X.-M.; Funakoshi, K.; Sakai, K. *Tetrahedron* **1991**, *47*, 4879–4888.
(43) Kundu, K.; McCullagh, J. V.; Morehead, A. T., Jr. *J. Am. Chem. Soc.* **2005**, *127*, 16042–16043.
(44) Fairlie, D. P.; Bosnich, B. *Organometallics* **1988**, *7*, 946–954.
(45) Koga, N.; Morokuma, K. *Chem. Rev.* **1991**, *91*, 823–842.
(46) Niu, S.; Hall, M. B. *Chem. Rev.* **2000**, *100*, 353–405.
(47) Torrent, M.; Sola, M.; Frenking, G. *Chem. Rev.* **2000**, *100*, 439–493.
(48) Ziegler, T. *Chem. Rev.* **1991**, *91*, 651–667.
(49) Ziegler, T.; Autschbach, J. *Chem. Rev.* **2005**, *105*, 2695–2722.
(50) Chung, L. W.; Wu, Y.-D. *J. Theor. Comput. Chem.* **2005**, *4* (Spec. Issue), 737–749.

Scheme 2. Bosnich's Postulated Mechanism for Deuterium Scrambling during Rhodium-Catalyzed Hydroacylation

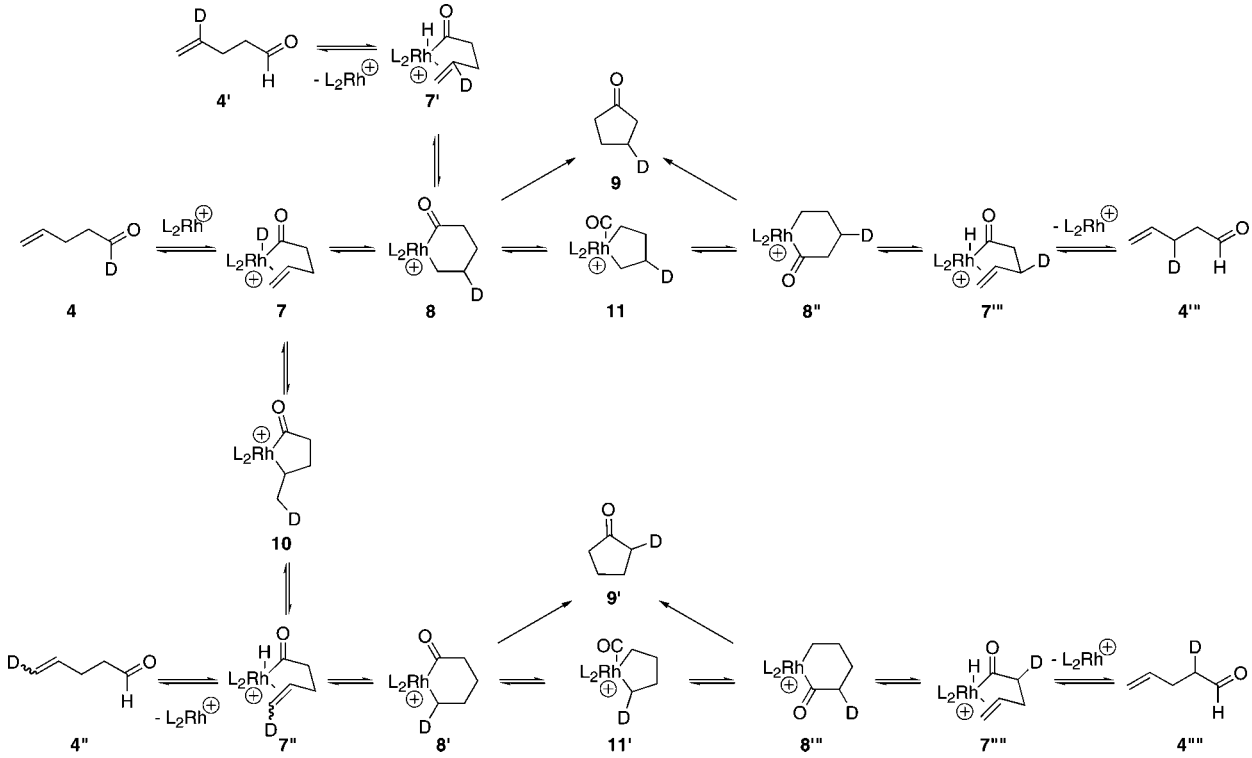

Scheme 3. Potential Decarbonylation Pathways

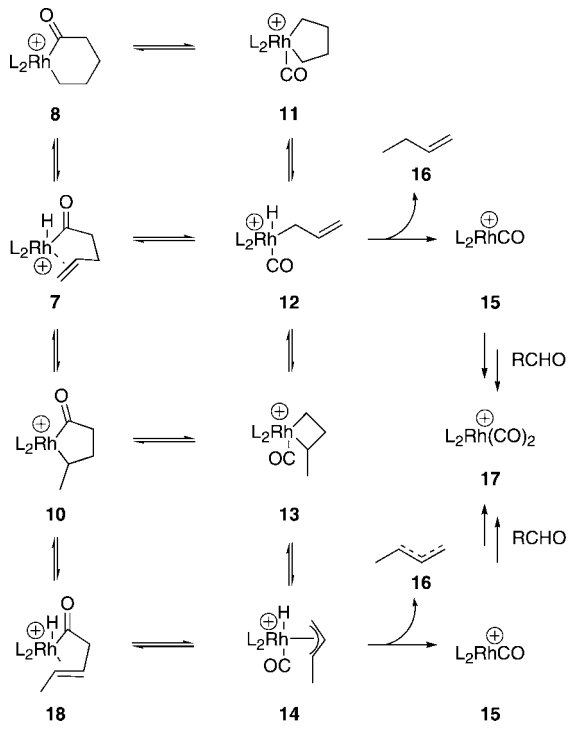

sponding to the analysis of the gas-phase reaction are presented, highlighting the oxidative addition step as the critical branch point for the important paths of the reaction. From these paths, the routes leading to product, decarbonylation, and isotopic scrambling are presented.

Next, results from the inclusion of explicit molecules of solvent or substrate are presented as the simplest possible approximation to modeling the reaction environment, focusing on the issues of coordinative unsaturation prevalent in the organometallic cycle rather than on the field effects of bulk solvation. Motivating these efforts is a well-documented dependence of reaction rate on the solvent in the rhodium-catalyzed transformation of 4-pentenal to cyclopentanone.[1,44] Numerical instabilities encountered with the implementation of standard reaction field approximations in the software we used prevented us from studying the effects of bulk solvation on the reaction. However, the explicit molecule model of the reaction environment facilitates an accurate treatment of the interaction between secondary molecules and coordinately unsaturated intermediates—species that are omnipresent in catalytic organometallic cycles. Specifically, the impact of the explicit molecules on the structures and energetics of the stationary points along the reaction paths is presented.

A brief discussion follows of the differences and similarities between our results and those from a recently reported computational study of a related reaction.

Finally, a brief comparison of our results to those calculated with a popular version of the QM/MM approach is presented.

2. Computational Methods

Energies, optimized equilibrium and transition-state geometries, and harmonic frequencies were calculated with the density functional software package DMol3.[51,52] The Becke−Tsuneda−Hirao gradient-corrected functional[53,54] was used along with double numerical plus polarization basis sets, a 20 bohr cutoff, fine integration grid, and scalar relativistic corrections[55] in the calculations presented herein. Default convergence criteria of 10^{-6} hartrees for the SCF and 10^{-3} hartrees/bohr for the gradient in geometry optimizations were employed.

Transition-state searches began from either QST estimates or nudged elastic band[56] calculations of the minimum energy paths.

(51) Delley, B. *J. Chem. Phys.* **1990**, *92*, 508–517.
(52) Delley, B. *J. Chem. Phys.* **2000**, *113*, 7756–7764.
(53) Becke, A. D. *J. Chem. Phys.* **1988**, *88*, 1053–1062.
(54) Tsuneda, T.; Hirao, K. *Chem. Phys. Lett.* **1997**, *268*, 510–520.
(55) Delley, B. *Int. J. Quantum Chem.* **1998**, *69*, 423–433.

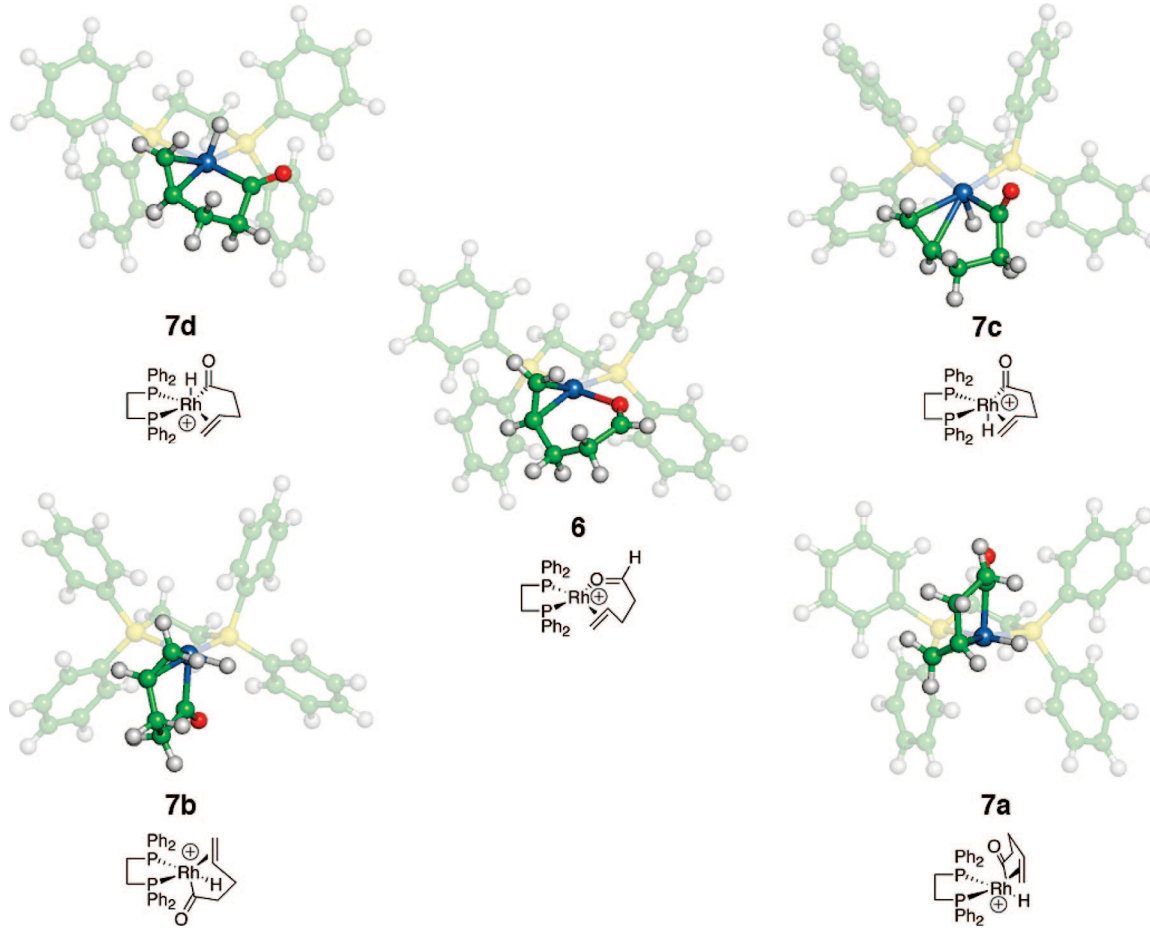

Figure 1. Optimized molecular geometries of the four possible isomers of **7** resulting from the intramolecular oxidative addition of **6**. Figure 2 lists the energies in kcal/mol, relative to **6**. The substrate/Rh portion of each complex is highlighted for clarity. Isomer **7d** is not stable at the highest level of theory applied in this study.

In both cases, subsequent transition-state optimizations were run to convergence, and frequency calculations were performed to confirm the presence of a single imaginary frequency. A nudged elastic band calculation or an animation of the imaginary frequency was utilized to substantiate the association of the transition-state structure with the intermediates on opposite sides of the reaction path.

Calculations approximating the solvent reaction field were attempted with the conductor-like screening model (COSMO).[57–59] The recommended default grid size (1082) was utilized, while the number of segments varied from the default of 92 up through 272 and 642. Despite these variations, numerical instabilities related to the complexity of the calculated solvent-accessible surface in the COSMO algorithm within DMol3 prevented the calculations from running successfully for all species along a given reaction path.

Binding energies were evaluated as the difference in energy between the optimized complex and the sum of the optimized free fragments.

For comparison, hybrid QM/MM calculations were performed via the two-layer ONIOM approach,[60,61] as implemented in Gaussian03.[62] All atoms that were not part of the four phenyl groups comprised the QM core, while the phenyls made up the MM periphery. All structures were optimized with the (B3LYP/LANL2DZ:UFF) method.

3. Results and Discussion

Gas-Phase Reaction Mechanism. Of central importance to the overall reaction mechanism is the demarcation of the reaction pathway at the oxidative addition step. Four diastereomers of **7** are possible from the intramolecular oxidative addition of **6**: two with the hydride apical and two with the acyl group apical (see Figure 1). Interestingly, both of the isomers with the acyl group apical are lower in energy than those that possess the

(56) Alfonso, D. R.; Jordan, K. D. *J. Comput. Chem.* **2003**, *24*, 990–996.
(57) Klamt, A. *J. Chem. Phys.* **1995**, *99*, 2224–2235.
(58) Klamt, A.; Jonas, V. *J. Chem. Phys.* **1996**, *105*, 9972–9981.
(59) Klamt, A.; Schueuermann, G. *J. Chem. Soc., Perkin Trans. 2* **1993**, 799–805.
(60) Maseras, F.; Morokuma, K. *J. Comput. Chem.* **1995**, *16*, 1170–1179.
(61) Svensson, M.; Humbel, S.; Froese, R. D. J.; Matsubara, T.; Sieber, S.; Morokuma, K. *J. Chem. Phys.* **1996**, *100*, 19357–19363.
(62) Frisch, M. J.; Trucks, G. W.; Schlegel, H. B.; Scuseria, G. E.; Robb, M. A.; Cheeseman, J. R.; Montgomery, J.J. A.; Vreven, T.; Kudin, K. N.; Burant, J. C.; Millam, J. M.; Iyengar, S. S.; Tomasi, J.; Barone, V.; Mennucci, B.; Cossi, M.; Scalmani, G.; Rega, N.; Petersson, G. A.; Nakatsuji, H.; Hada, M.; Ehara, M.; Toyota, K.; Fukuda, R.; Hasegawa, J.; Ishida, M.; Nakajima, T.; Honda, Y.; Kitao, O.; Nakai, H.; Klene, M.; Li, X.; Knox, J. E.; Hratchian, H. P.; Cross, J. B.; Bakken, V.; Adamo, C.; Jaramillo, J.; Gomperts, R.; Stratmann, R. E.; Yazyev, O.; Austin, A. J.; Cammi, R.; Pomelli, C.; Ochterski, J. W.; Ayala, P. Y.; Morokuma, K.; Voth, G. A.; Salvador, P.; Dannenberg, J. J.; Zakrzewski, V. G.; Dapprich, S.; Daniels, A. D.; Strain, M. C.; Farkas, O.; Malick, D. K.; Rabuck, A. D.; Raghavachari, K.; Foresman, J. B.; Ortiz, J. V.; Cui, Q.; Baboul, A. G.; Clifford, S.; Cioslowski, J.; Stefanov, B. B.; Liu, G.; Liashenko, A.; Piskorz, P.; Komaromi, I.; Martin, R. L.; Fox, D. J.; Keith, T.; Al-Laham, M. A.; Peng, C. Y.; Nanayakkara, A.; Challacombe, M.; Gill, P. M. W.; Johnson, B.; Chen, W.; Wong, M. W.; Gonzalez, C.; Pople, J. A. *Gaussian 03, Revision D.01, Gaussian 03, Revision D.01*; Gaussian, Inc: Wallingford, CT, 2004.

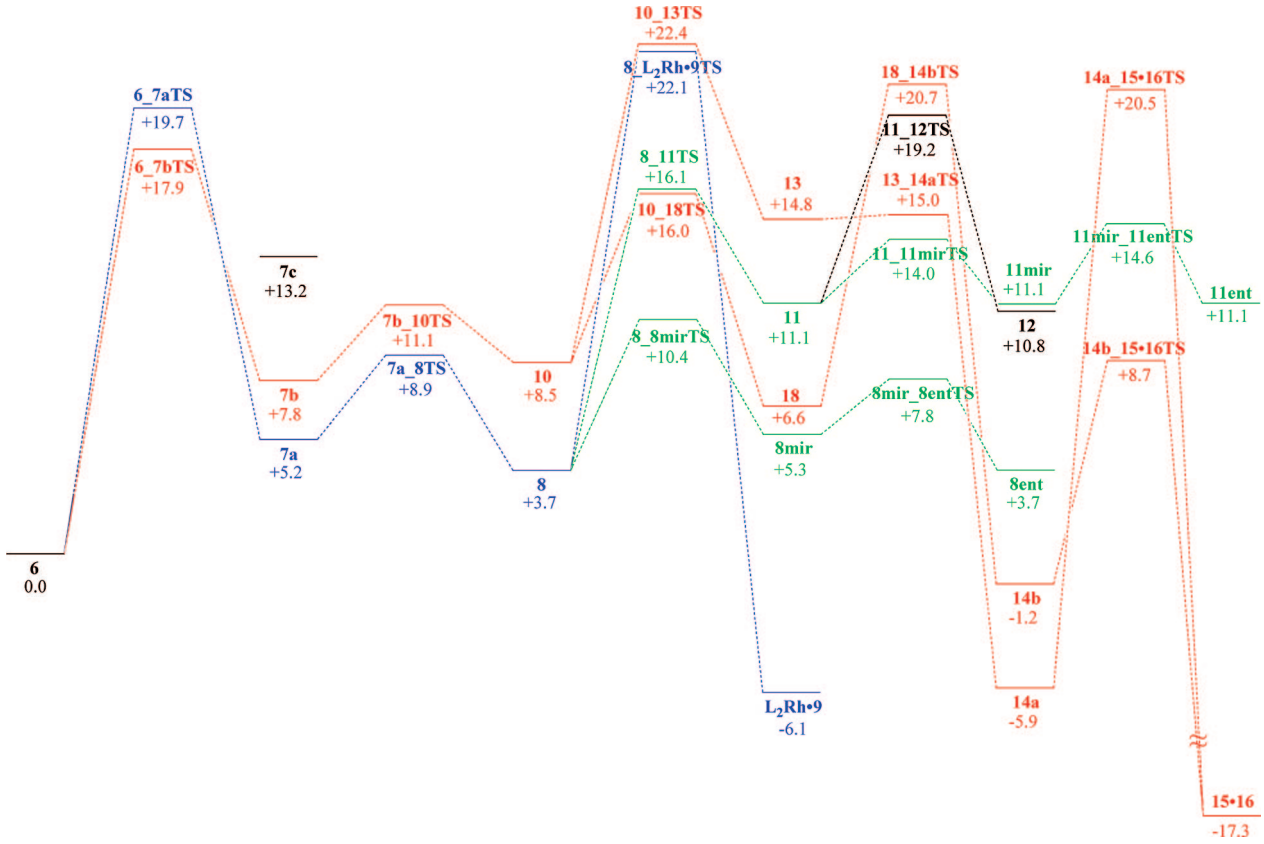

Figure 2. Calculated energies (kcal/mol), relative to **6**, for the gas-phase intramolecular hydroacylation reaction. Color coding of pathways: blue, productive path leading to cyclopentanone; red, effective decarbonylation; green, isomerization/scrambling.

hydride apical. This is counter to the typical order known for the trans influence of ligands[63] and has significant implications for the catalytic pathway, which will be discussed below.

Note that both **7a** and **7b** are significantly lower in energy than **7c** (by approximately 8.0 and 4.5 kcal/mol, respectively); structure **7d** must be regarded as hypothetical, since it is not stable when scalar relativistic corrections are included in the computation. In the absence of such corrections, **7d** is +23.2 kcal/mol higher than **6**. We can only attribute this stereochemical preference to a higher trans influence for the acyl ligand relative to the hydride, since no other discernible differences in bond lengths or geometries are evident. This preference was previously noted by Chung and Wu in their related computational study, although they did not comment on the observation.[50] We are currently investigating this interesting phenomenon and anticipate publishing a follow-up communication.

Note, too, that the Rh(III) intermediates **7a**−**c** have flipped their diphos ligands from a local C_2 symmetry to C_s, which appears to open a wedge of reactivity while blocking access to the empty coordination site opposite the apical ligand. Many common bidentate and/or asymmetric ligands are incapable of this inversion of stereochemistry at one phosphine, suggesting a potential strategy for accelerating catalysis with nonsymmetric ligands designed to utilize this change. While it is tempting to attribute the C_2 to C_s interconversion of the diphos ligand to the greater size of the acyl, the apical hydride structure (**7c**) also has the phosphine phenyl groups rotated in an analogous manner.

All of the structures presented in this study can exist in two different helical conformations due to the stagger of the ethylene bridge of diphos. We have maintained a single enantiomeric series throughout our reaction paths, with the exception of processes that must access the other enantiomer via isomerization. Those structures will be indicated with the nomenclature **ent**.

Scheme 4. Catalytic Cycle for Hydroacylation with the Acyl Group Apical Following Oxidative Addition

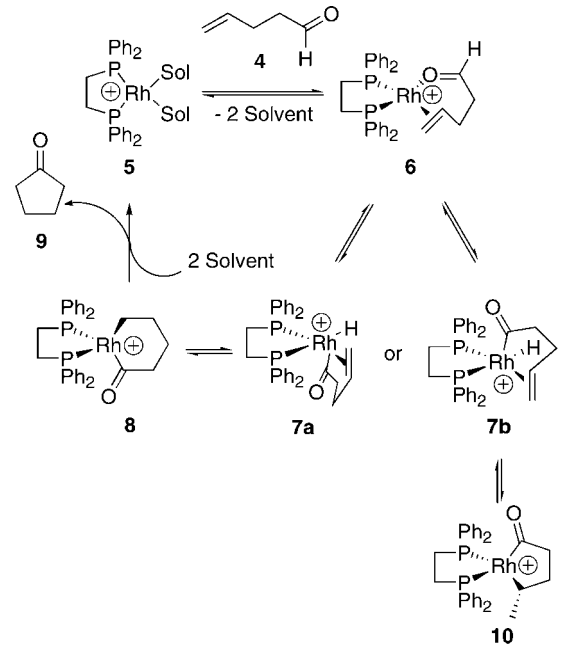

The most important consequence of the stereochemical branch point defined by the oxidative addition step is that **7**, **8** and **10**, shown in Scheme 1, are not on the same pathway. According

(63) Atwood, J. D. *Inorganic and Organometallic Reaction Mechanisms*; VCH: Weinheim, 1985; 312pp.

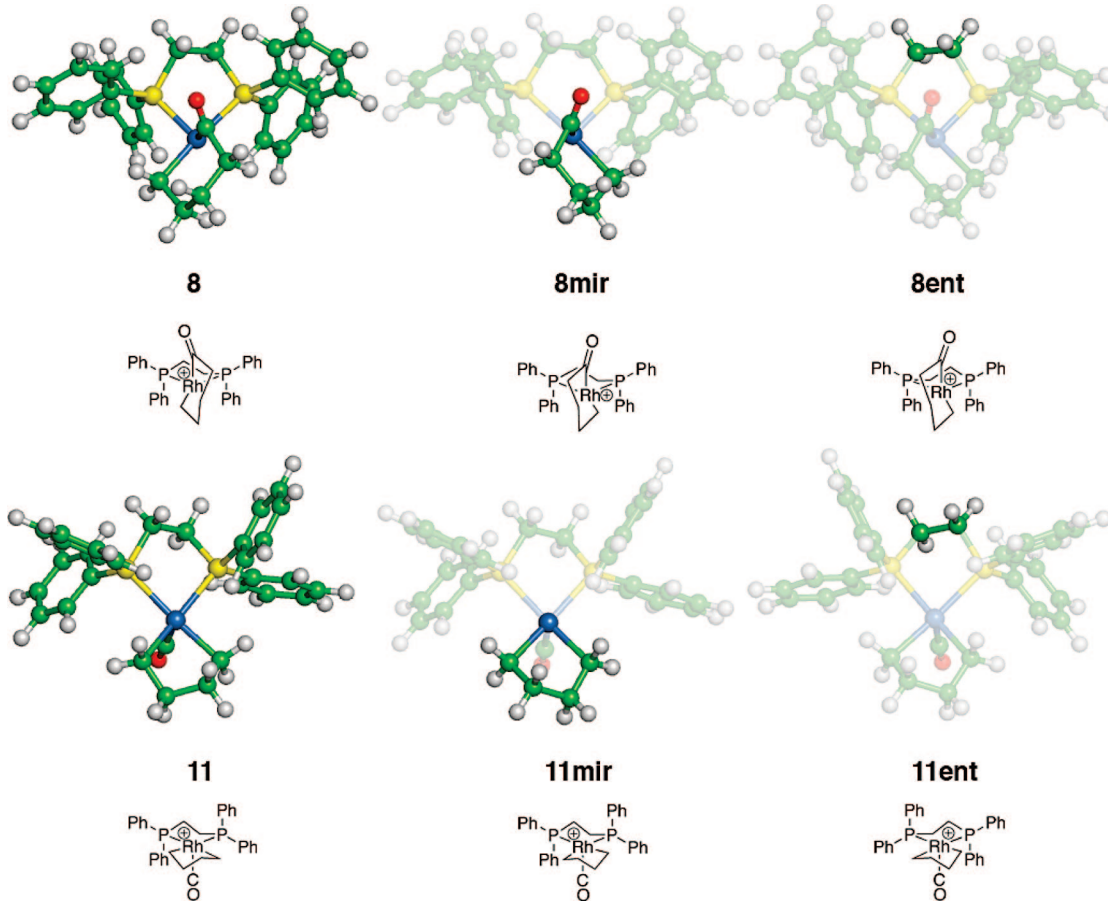

Figure 3. Optimized molecular geometries of **8** → **8mir** → **8ent**, and **11** → **11mir** → **11ent**, highlighting the key geometric change in each isomerization step.

to Scheme 1, the mechanism proceeding through 1,2 insertion from **7** formed **8** and 2,1 insertion formed **10**. It is now clear that the 1,2 and 2,1 insertions take place from different isomers of **7**, with **7a** leading to **8** and **7b** leading to **10**. Thus, to interconvert **8** and **10**, the reaction must reverse to **6**, as shown in Scheme 4. With the apical hydride (**7c**), insertion leads to a different metallocycle—an isomer of **8** in which both the acyl and alkyl are equatorial, but with a barrier that is unrealistically high in energy (+30.1 kcal/mol, not shown in Figure 2). As such, it was omitted from further consideration.

The calculated reaction coordinate for the entire catalytic cycle, including important side reactions, is shown in Figure 2. As discussed above, intermediates **7a** and **7b** are on separate pathways. The formation of intermediates **8** and **10** from **7a** and **7b** are low barrier processes and are readily reversible. Further, the hydride migrates to the alkene in this step, rather than the alkene inserting into the metal—hydride bond.

Unsurprisingly, intermediates **8** and **10** proceed to different products. The productive pathway from **8** involves reductive elimination to give cyclopentanone coordinated to the rhodium catalyst, $\mathbf{L_2Rh \cdot 9}$, at which point exchange with pentenal will regenerate **6**. Intermediate **8** will also proceed down two other pathways. The first involves a ring flip, inverting the metallocyclohexanone to yield the local mirror image, **8mir**, followed by inversion of the ethylene bridge of the diphos ligand to generate the enantiomer, **8ent** (see Figure 3). Both barriers in this process are low energy (+6.7 and 2.5 kcal/mol, respectively), and the transformation is of importance primarily in understanding the labeling results (vide infra). The other pathway involves carbonyl deinsertion to give **11**. Two low

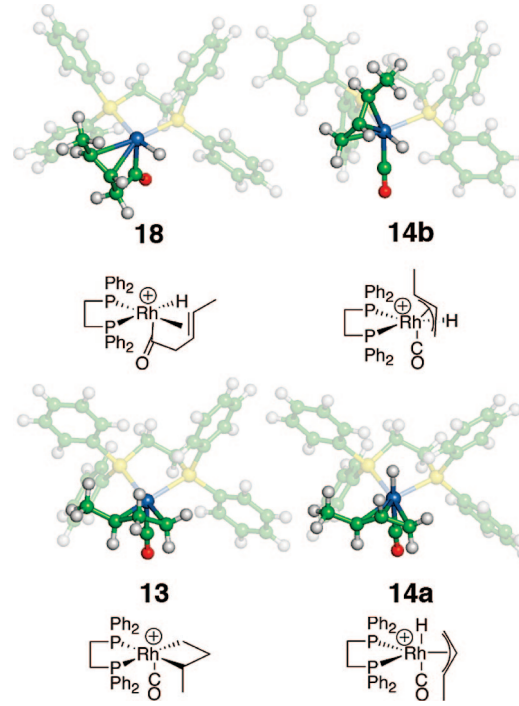

Figure 4. Key intermediates **18**, **14b**, **13**, and **14a** along the catalyst deactivation/decarbonylation pathways.

energy pathways proceed from **11**; isomerization to the enantiomer, **11ent** (also via **11mir**) and β-hydride elimination to yield **12**. Reductive elimination from **12** to **15**·**16** passes through

Scheme 5. Isotope Scrambling Mechanisms with the Acyl in the Apical Position (the Conformations of the Ligand Backbone Are Not Shown for Clarity)[a]

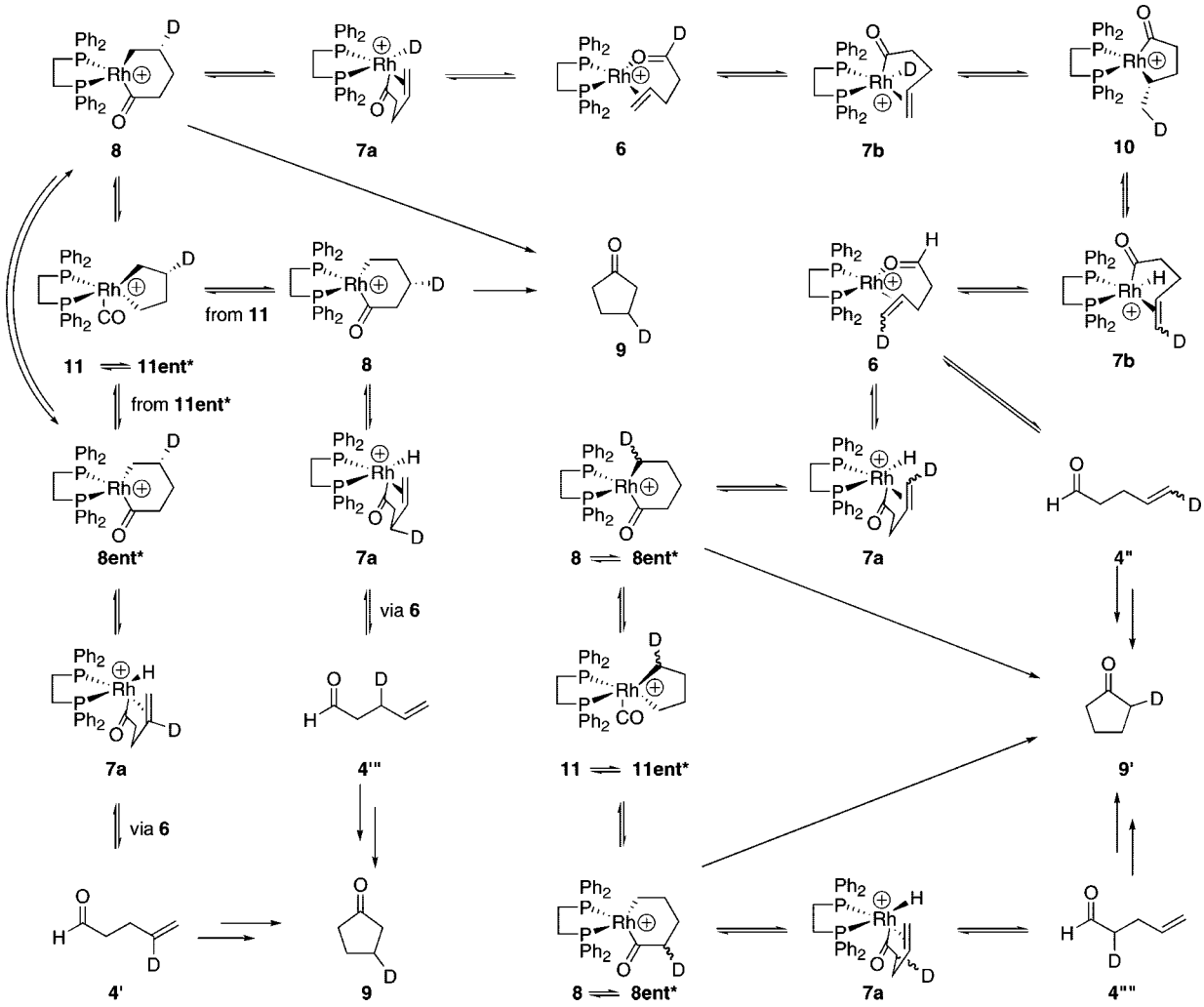

[a] In addition, with the stereocenter created by the deuterium, **8ent*** and **11ent*** are diastereomers of **8** and **11** (rather than enantiomers); we have retained the **ent** nomenclature to correspond with Figures 2 and 3.

a prohibitively high barrier at +29.9 kcal/mol, and is therefore not shown in Figure 2. As such, **12** is not part of a viable decarbonylation pathway that leads to catalyst decomposition, a result that stands in contrast to the pathway **7** → **12** → **15** + **16** proposed by Bosnich.

The primary pathway for **10**, aside from reversal to complex **6**, is β-hydride elimination to give **18**, followed by carbonyl deinsertion to yield **14b**, which then reductively eliminates rapidly to give 1- or 2-butene (**16**) and the monocarbonyl rhodium complex **15**. A competitive pathway exists in which carbonyl deinsertion from **10** takes place first, yielding **13**, followed by β-hydride elimination (**14a**) and, ultimately, reductive elimination to 1- or 2-butene (**16**) and the monocarbonyl rhodium complex **15**. Key structures from both pathways are illustrated in Figure 4. The pathway through **13** possesses a higher barrier than that through **18** (22.4 kcal vs 20.7 kcal). In addition, intermediate **18** is more stable than **13**, which likely favors the pathway through which it evolves, since **14a** and **14b** are geometric isomers and are both more stable than **10**. As such, the discussion that follows will focus only on the **10** → **18** → **14b** → **15**•**16** decarbonylation pathway.

Deuterium Scrambling. Illustrated in Scheme 5 are the pathways, consistent with our calculations, which account for the scrambling products observed experimentally. The primary difference between the pathway proposed by Bosnich (Scheme 2) and that in Scheme 5 is that **10** is not an intermediate through which the two major pathways can interconvert. Once **10** is formed, it will result in the formation of **4**″ and **4**″″. Structure **10** is not an intermediate on the pathway that gives **4**′ and **4**‴, both of which are instead derived from **8**.

It is interesting to note that **4**′ can only be derived from **8ent**, which may be formed by isomerization of **8** (via **8mir**) or from **11** to **11ent** and back to **8ent** (Figure 3). Both pathways have relatively low barriers but are still slow enough that **4**′ is the minor product of the four isotopically labeled starting materials observed. Without isomerization to **8ent**, deinsertion of **8** simply removes the deuterium and returns to **6**. In contrast, **4**‴ is formed by a straightforward pathway proceeding from **8** to **11** and back to **8** (or the same pathway via **8ent** or **11ent**) then reinserting into the other alkyl Rh-C bond, and is thus formed more readily.

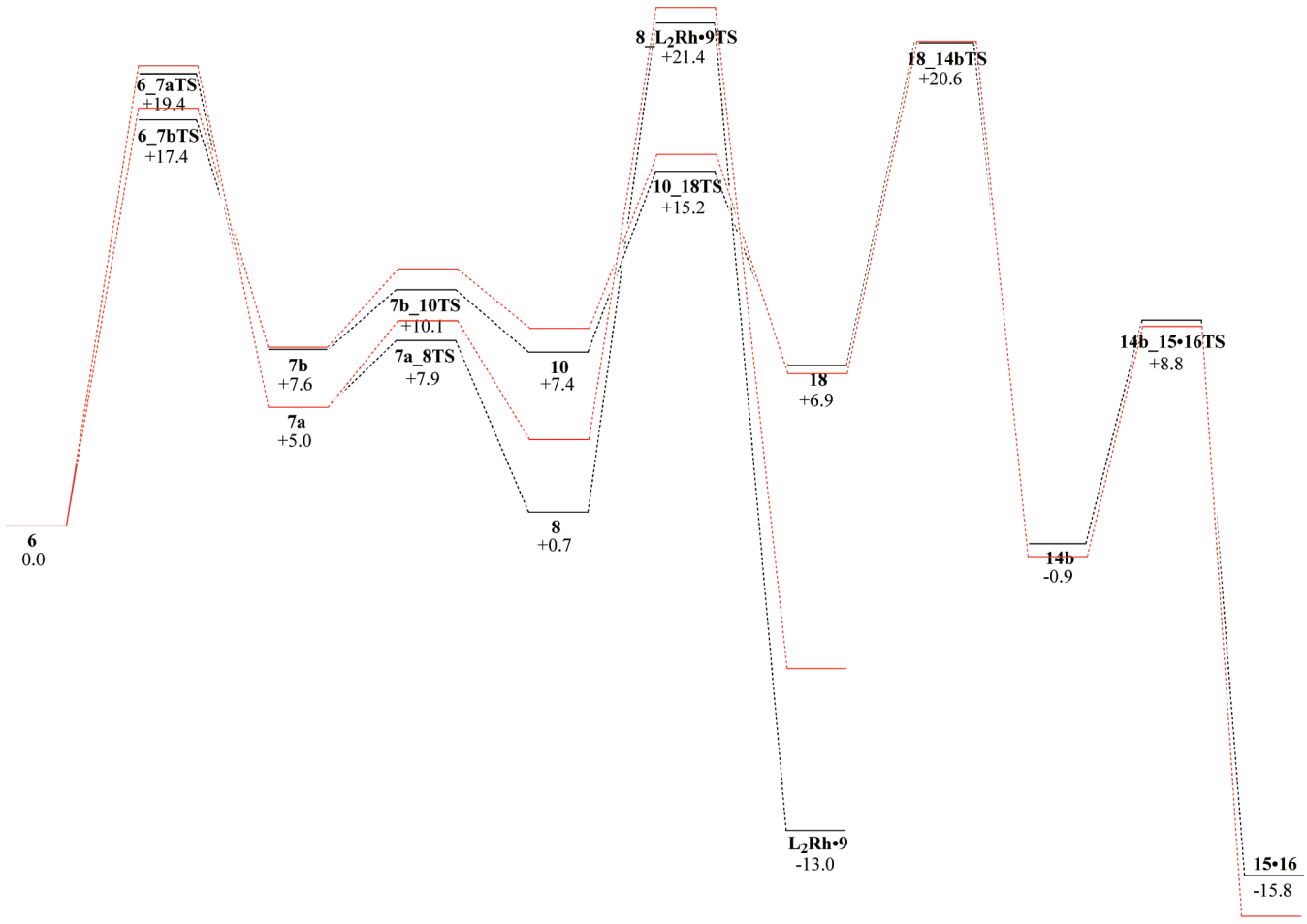

Figure 5. Calculated energies (kcal/mol), relative to **6**, for the reaction profile in the presence of an explicit molecule of nitromethane (black). Overlain (in red) is the gas-phase reaction profile of the corresponding species.

Isomer **4′′′′**, much like isomer **4′**, requires the isomerization of **8ent** or **11** to **11ent**, the deinserted intermediate, followed by CO reinsertion into the other Rh-C bond. It, too, will be formed less readily than isomer **4′′**, since **4′′** requires no inversion of the substrate metallocycle or the ethylene bridge of the chelating diphos. With two major pathways, one of which cannot reductively eliminate to product (**7b** → **10** → **18**), the others of which possess relatively low energy barriers compared with the energy required for reductive elimination to form product, scrambling is facile.

Coordination Effects. While the calculated mechanism shown in Figure 2 illustrates two major pathways that can explain many of the results reported by Bosnich, several significant issues remain that are not adequately explained, and include the following:

• The rate of decarbonylation, and therefore catalyst deactivation, is predicted from Figure 2 to be faster than the rate of reductive elimination leading to product formation.

• Open coordination sites are present in many of the rhodium (III) complexes, a fact that may not persist in the condensed phase with even weakly coordinating solvent.

• Bosnich noted that turnover rate decreased with increased substrate concentration while at the same time turnover numbers increased.

These issues are either unsupported by the experimental results (first bullet) or are unaccounted for in the gas-phase reaction mechanism illustrated in Figure 2 (bullets two and three). Such discrepancies need to be reconciled. Clearly, an approximation of the environment—solvation and additional substrate—must be included in the model.

Solvation has long been an issue of significant importance in computational chemistry,[64] and our intent in this study was to apply a two-pronged approach to model the environment in this system. The first was to employ Klamt's Conductor-like Screening Model (COSMO),[57–59] which is an excellent tool for evaluating the energetic and geometric response of a molecule in the presence of a solvent dielectric continuum. The second part of our approach would focus on coordination effects by explicitly including molecules of substrate or solvent in the geometry optimization step. Previous work has demonstrated that the addition of a small number of explicit molecules is sufficient to recover certain bulk thermodynamic properties of the condensed phase.[65] Other work combines QM/MM methods with molecular dynamics to improve the explicit-molecule approximation to solvation.[66]

As discussed in the Computational Methods, the COSMO algorithm did not yield results for all steps of the reaction mechanism. However, we were able to establish that the basic trends in energetic stabilization of intermediates and transition states exhibited by including a single explicit molecule of solvent mimicked, to a limited extent, those from the successful

(64) Tomasi, J. *Theor. Chem. Acc.* **2004**, *112*, 184–203.
(65) Glendening, E. D.; Feller, D.; Thompson, M. A. *J. Am. Chem. Soc.* **1994**, *116*, 10657–10669.
(66) Woo, T. K.; Blochl, P. E.; Ziegler, T. *THEOCHEM* **2000**, *506*, 313–334.

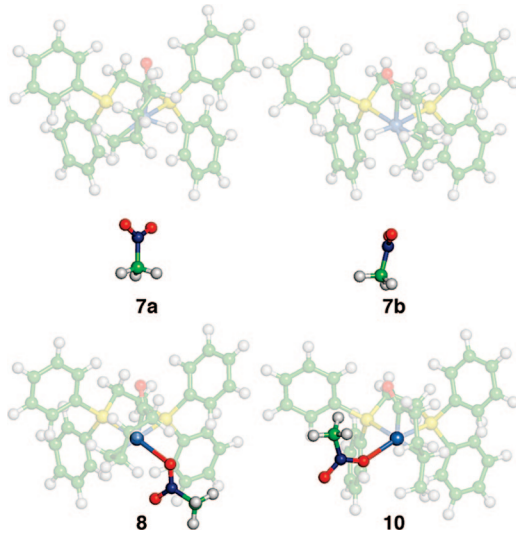

Figure 6. Molecular geometries of intermediates **7a**, **7b**, **8**, and **10**, optimized in the presence of a molecule of nitromethane. Highlighting emphasizes the inner-sphere coordination of nitromethane in the latter two.

COSMO calculations. The explicit molecule approach sought to address the coordinative unsaturation that existed in many steps of the calculated catalytic cycle. In this context, we explored the impact of three different molecules, each added separately, on the reaction profile: nitromethane (solvent, very weakly coordinating), acetone (solvent, strongly coordinating), and 4-pentenal (substrate, modestly coordinating).

Figure 5 shows the calculated energies in the presence of a single molecule of nitromethane and, for comparison, overlays the gas phase results from Figure 2. The significant differences are relatively few in number: the overall profile remains as discussed above, yet intermediates **8**, **10**, and **L_2Rh•9** exhibit a substantial degree of energetic stabilization. In all three cases, each is significantly stabilized relative to the energy in the absence of nitromethane.

Inspection of the geometric structures of these intermediates reveals the origin of the stabilization. All three involve coordination of an oxygen of nitromethane to the rhodium, demonstrating how even a weakly coordinating ligand can stabilize coordinatively unsaturated complexes. Importantly, as shown in Figure 6, intermediates **7a** and **7b** do not coordinate nitromethane in the inner coordination sphere due to the steric bulk of the phenyls on the phosphines blocking the open site and thus are not significantly stabilized.

Note that although the transition state for reductive elimination (**8_L_2Rh•9TS**) is still higher in energy (by 0.8 kcal/mol) than the transition state leading down the decarbonylation pathway (**18_14bTS**), the former is lowered considerably (−0.7 kcal/mol) relative to the latter (−0.1 kcal/mol) in the presence of nitromethane. This observation implies that coordination may play a role in accelerating catalysis and underscores the need to investigate more strongly coordinating species.

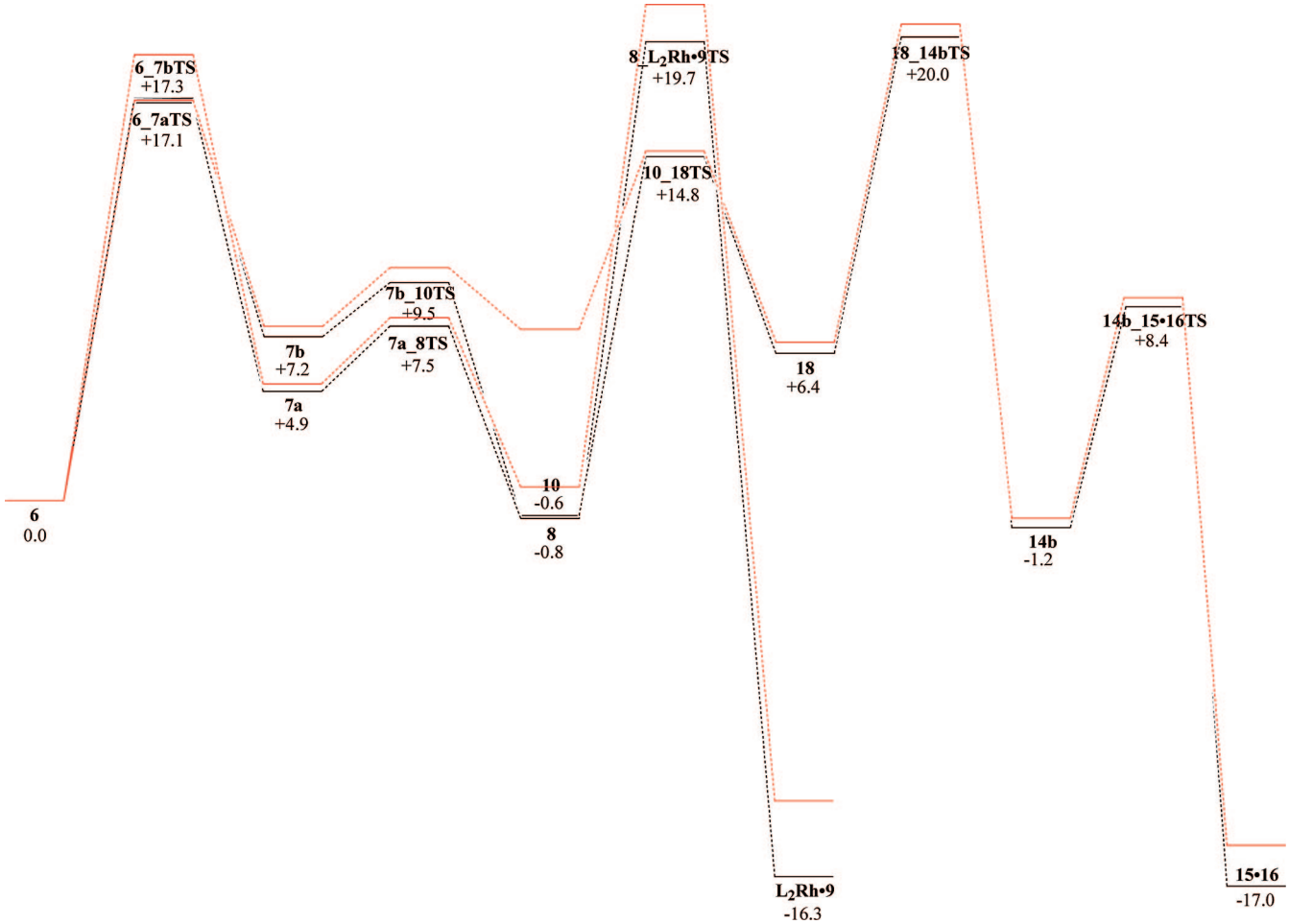

Figure 7. Calculated energies (kcal/mol), relative to **6**, for the reaction profile in the presence of an explicit molecule of acetone (black). Overlain (in red) is the reaction profile in the presence of an explicit molecule of nitromethane.

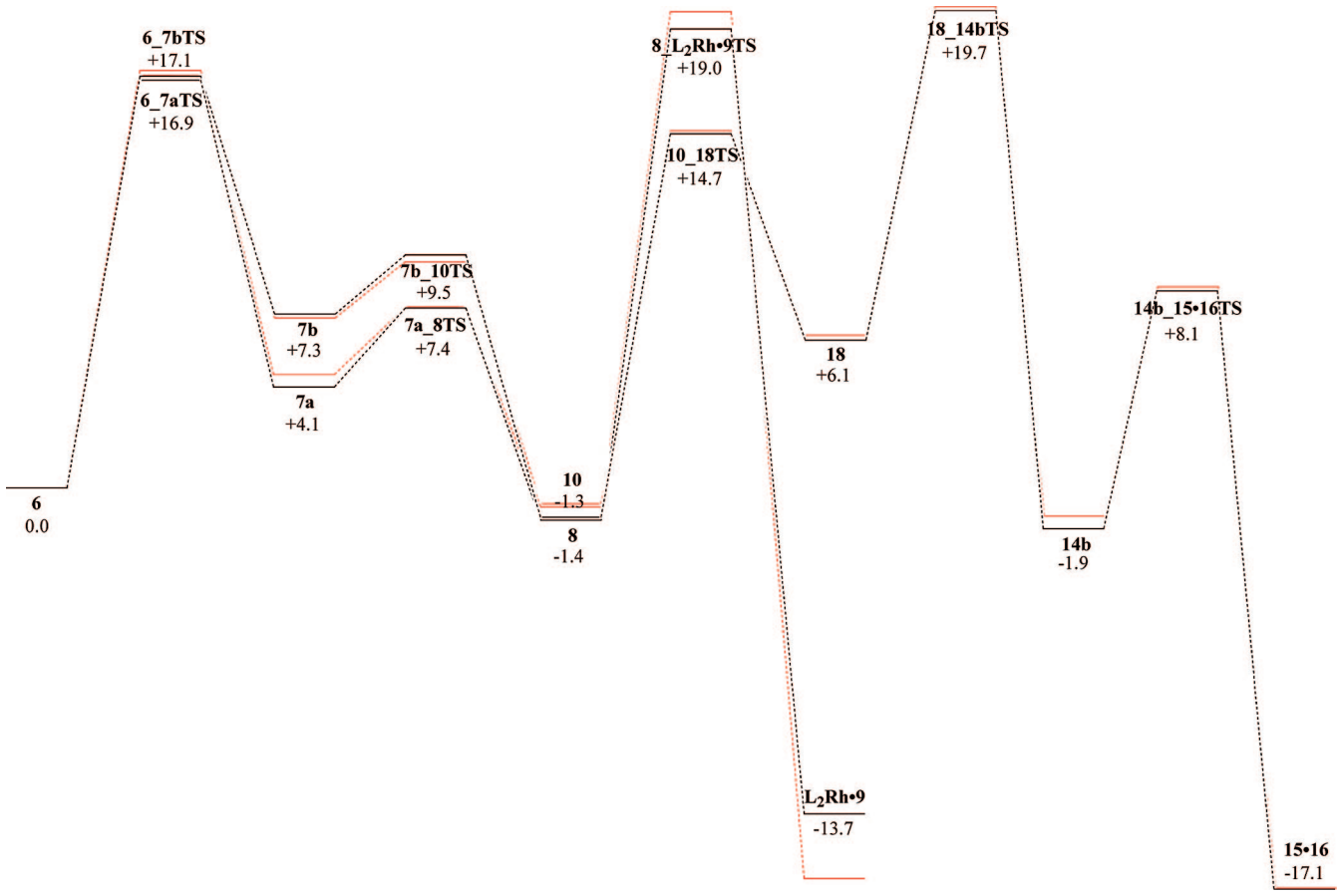

Figure 8. Calculated energies (kcal/mol), relative to **6**, for the reaction profile in the presence of an explicit molecule of 4-pentenal (black). Overlain (in red) is the reaction profile in the presence of an explicit molecule of acetone.

Shown in Figure 7 is the overlay of the reaction profiles of nitromethane and acetone. One key result is that **10** is preferentially stabilized by acetone relative to **8**, so much so that it is nearly degenerate with **8**. Inspection of the structures shows that while **10** more closely coordinates acetone (2.200 vs 2.302 Å for the Rh−O bond), a close contact between one of the methyls of acetone and the acyl carbon of the ligand offsets the stabilization that is due to the stronger Rh−O bond. Although the transition state leading to reductive elimination experiences greater stabilization with acetone than with nitromethane, the transition states and corresponding intermediates on the decarbonylation path are stabilized as well. Note that the transition state for decarbonylation is now just above that of reductive elimination, consistent with the observation that decarbonylation occurs relatively rapidly in acetone when compared with nitromethane or dichloromethane.

Another significant difference occurs in the oxidative addition transition state, where the gap of ca. 2 kcal/mol seen in the presence of nitromethane and in the gas phase has been reduced to 0.2 kcal/mol. It is interesting that significant stabilization occurs without coordination of the ligand to the metal. We attribute this stabilization to the charge−dipole interaction between the solvent and the rhodium cation, and this observation helps explain why addition of a single molecule of solvent or second mole of substrate recovered a portion of the stabilization observed in the COSMO calculations (vide supra).

Figure 8 shows an overlay of the reaction coordinates with explicit acetone and explicit second molecule of substrate included. Of primary importance is the result that the transition state for reductive elimination in the presence of an additional molecule of 4-pentenal has dropped further below that of the decarbonylation pathway. Athough acetone is a more strongly coordinating ligand, the Rh−O bond distances are remarkably similar in **8**: for acetone it is 2.275 Å and for pentenal it is 2.280 Å. In the square-planar $\mathbf{L_2Rh \cdot 9}$ products, where there is less steric congestion, the Rh-O bond distances are 2.239 and 2.224 Å for pentenal and acetone, respectively. As the reaction evolves through the transition state for reductive elimination, the steric congestion at the reactive site persists, as supported by an analysis of energies associated with the exchange reaction shown in eq 3.

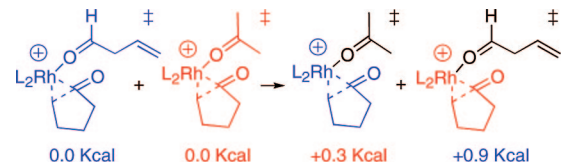

(3)

The structures on the left side of eq 3 represent the fully optimized transition states for reductive elimination (**8_L2Rh•9TS**) in the presence of explicit molecules of 4-pentenal (blue) and acetone (red). On the right, acetone and pentenal are exchanged and allowed to optimize under the constraint of fixed substrate + catalyst geometries. As the color-coding implies, the blue substrate + catalyst nuclear positions are those from the full optimization (blue on the left); the red positions for the pentenal optimization are those from the full acetone optimization (red on the left). The structure with acetone exchanged for pentenal is only 0.3 kcal/mol higher energy than its fully optimized counterpart, while the structure with pentenal exchanged for acetone is more dramatically destabilized (by 0.9 kcal/mol). Viewed in reverse, the latter system (pentenal at the

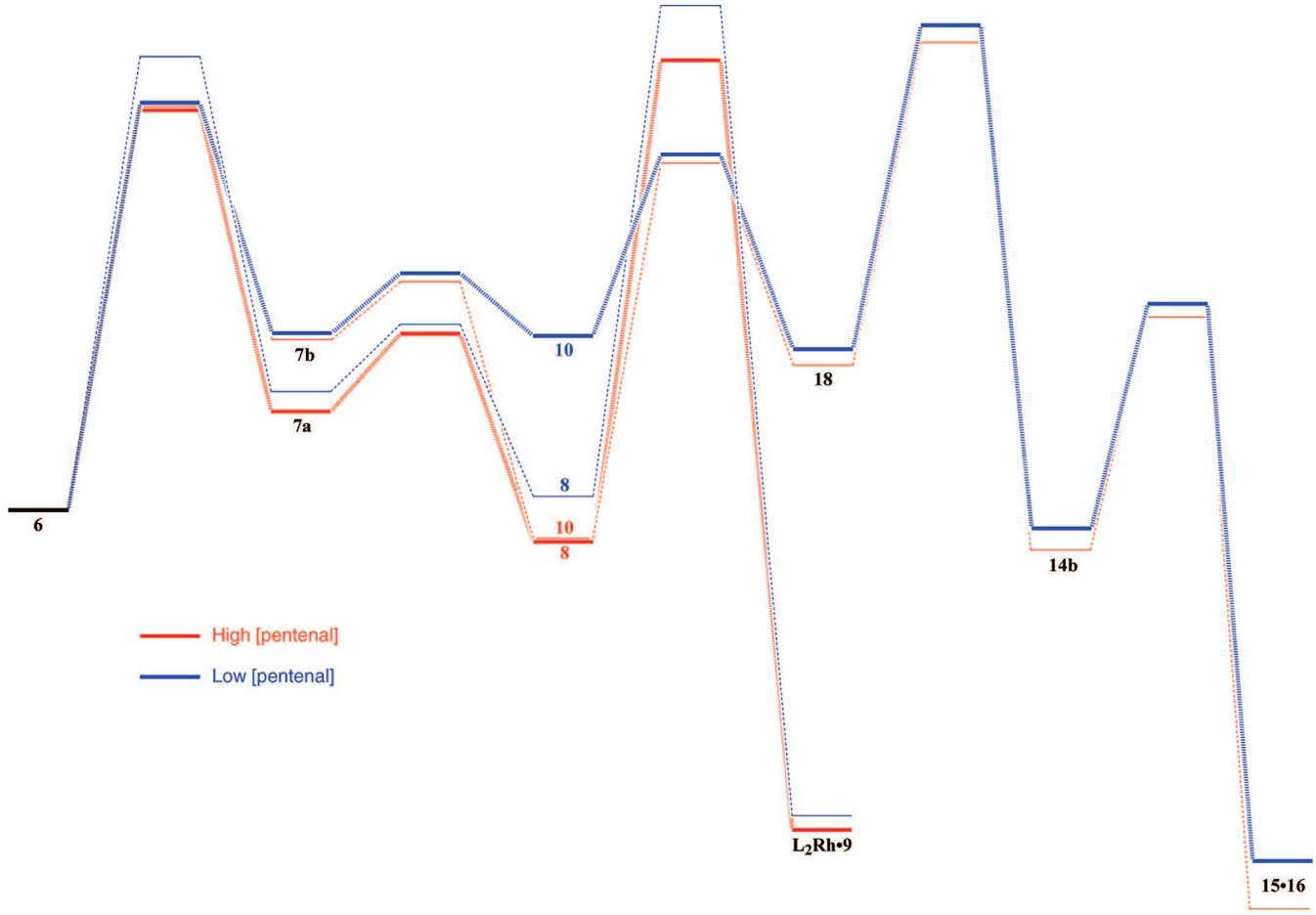

Figure 9. Overlay of reaction profiles involving explicit molecule of nitromethane (blue) and explicit molecule of 4-pentenal (red). Shown in bold are the productive pathway (red) at high concentrations of pentenal and the decarbonylation pathway populated at low concentrations of pentenal (blue).

acetone geometry) relaxes further and is evidence supporting a more congested, and hence less stable, transition state structure with coordinated acetone than that with pentenal.

From the perspective of normal catalysis, Figure 9 provides a comparison of the reaction profiles in nitromethane and the second mole of substrate. At higher concentrations of starting material, the primary (fastest) pathway involves reductive elimination (red **6** → **7a** → **8** → **product**). As the concentration of the aldehyde drops, the second pathway (blue **6** → **7b** → **10** → **18** → **14b** → **15·16**) becomes competitive and leads to catalyst death. These two limiting cases are represented by the profiles highlighted in Figure 9. At high concentrations of substrate the limiting case involves binding a second molecule of substrate. At low concentrations, the limiting case has the second molecule of substrate replaced by solvent.

Bosnich was therefore correct in asserting that filling a vacant coordination site with pentenal confers a protective effect, but not by preventing decarbonylation through blocking a vacant coordination site, but rather by accelerating the productive pathway. Support for this position comes from Fu, who observed in the hydroacylation reaction of 4-alkynals that addition of 10 equivalents of acetonitrile improved the yield of the reaction.[26] Both acetonitrile and the aldehyde are stericly unencumbered and have good σ coordinating ability and thus are likely candidates for this type of selective acceleration.

Finally, calculations support the role pentenal plays in inhibiting the reaction by nonproductive binding to the rhodium complex. This is illustrated in Figure 10. Depending on the relative coordinating ability and concentrations of the solvent and pentenal, the equilibrium illustrated in Figure 10 may shift in multiple ways. In a strongly coordinating solvent such as acetone, the catalyst exists predominately as the solvated **5**. An even stronger coordinating solvent such as acetonitrile could shut down catalysis due to the stability of **5**, an effect observed by Bosnich.

In a weakly coordinating solvent such as nitromethane (or dichloromethane), **20** and **6** are expected to be present in higher concentration. At higher concentrations of pentenal, **20** will be favored to a greater extent, decreasing the concentration of **6** and slowing the reaction. Shown in Table 1 are the calculated binding energies for various solvents coordinated to **5** and **19**, as well as the complexes **20**, **21** and **6**. Importantly, **6** and **20** have identical binding energies (to within the ±0.1 kcal/mol accuracy of the calculation) and are therefore interchangeable to participate in the equilibrium, thus slowing the reaction (since

Table 1. Binding energies (ΔE) of the Preequilibirum Species Shown in Figure 10

complex	binding energy (kcal/mol)
6	−34.4
5 (nitromethane)	−30.8
19 (nitromethane)	−31.6
5 (acetone)	−36.1
19 (acetone)	−35.4
5 (acetonitrile)	−41.8
20	−34.4
21	−31.2
22	−20.4

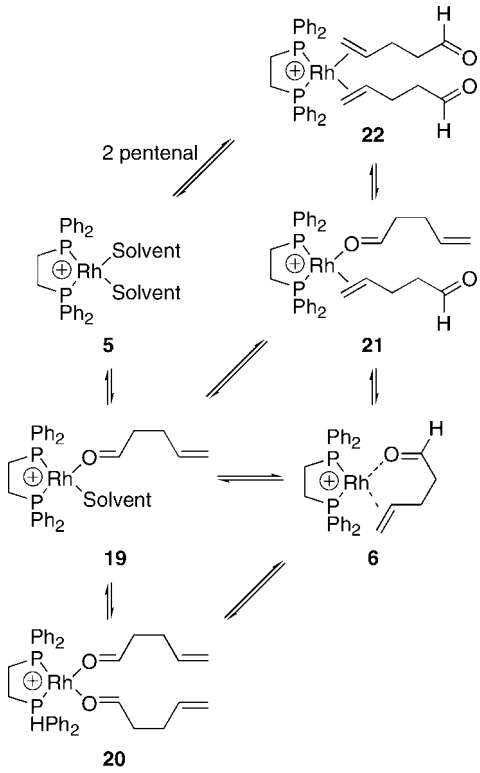

Figure 10. Substrate inhibition mechanism.

20 is unable to oxidatively add) at high substrate concentrations. As mentioned previously, acetonitrile and acetone bind more strongly, favoring **5**, the former to such an extent that catalysis is shut down. Interestingly, **21** and **22** are ca. 3 and 14 kcal/mol less stable than **6** and **20**, respectively, suggesting that alkene coordination does not play a major role in the reaction.

Comparison to Related Computational Work. A brief comparison with the previously reported work of Chung and Wu is in order. Chung and Wu modeled an alkyne as the unsaturated hydrocarbon in the intermolecular hydroacylation reaction (eq 4). They utilized a reasonable method and basis set (MP2//6-31G*/LANL2DZ); however, they had a significantly truncated system (no phenyl rings on the bidentate ligand) which means they would not have observed the steric effects that are very important in the system we have analyzed. In addition, our system involves an alkene, which undergoes less facile hydroacylation reactions.

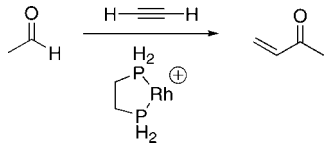

(4)

While Chung and Wu found oxidative addition to be the rate-limiting step, we found that reductive elimination was rate limiting. Wu found barrier heights of 27.9 kcal/mol for oxidative addition and 19.4 kcal/mol for reductive elimination; we found 16.9 kcal/mol for the oxidative addition and 19.0 kcal/mol for reductive elimination (with pentenal as second ligand). Both groups reliably found the apical acyl to be significantly more stable than the equatorial acyl following oxidative addition (Chung and Wu by nearly 10 kcal/mol).

Both groups found the insertion steps to possess a low barrier and proceed in a facile manner. Chung and Wu did not report a barrier for the intramolecular variant.

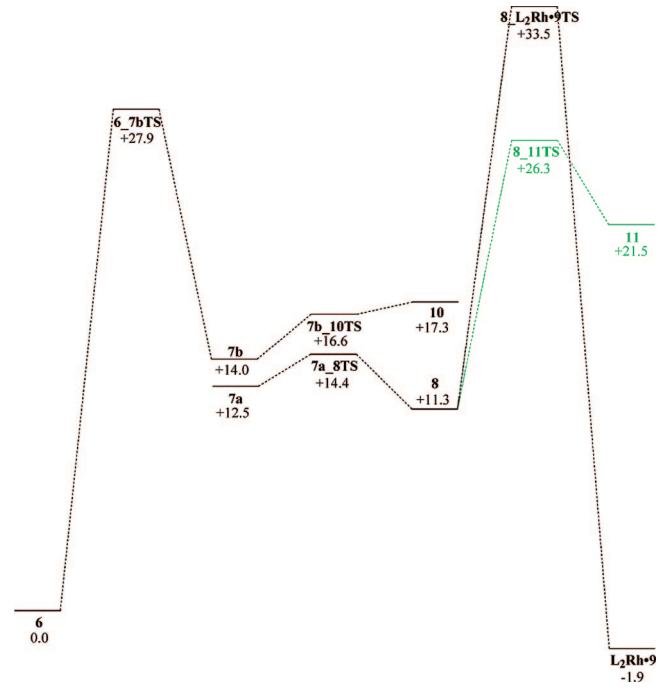

Figure 11. Calculated energies (kcal/mol) relative to **6**, obtained from the application of (B3LYP/LANL2DZ:UFF) QM/MM methods.

By contrast, the major issue in the Chung and Wu pathway was rapid decarbonylation relative to reductive elimination (barriers 10.0 kcal/mol vs 20.2 kcal/mol, respectively). Their proposed solution to this problem was to add a chelating group on the aldehyde, which blocks decarbonylation by filling the vacant coordination site. We found the barriers for the two pathways to be close together, and that variation of the equatorial ligand between solvent and pentenal could favor one pathway over the other.

Lastly, Chung and Wu determined that two alkynes strongly coordinated to the catalytically active species and was followed by dimerization. In contrast, we observed that the bis olefin complex **22** did not possess significant stability.

In summary, despite some fundamental differences between the present work and that of Chung and Wu (alkene vs alkyne substrate, full molecular model vs truncated model, reductive elimination vs oxidative addition as the rate determining step, comparable barriers for reductive elimination and decarbonylation vs significantly different barriers) both studies serve to elucidate key components of the hydroacylation reaction, albeit one for the intramolecular version, the other for the intermolecular.

Application of a QM/MM Method. Results from the application of a popular QM/MM method are shown in Figure 11. Although the reaction energetics are substantially exaggerated relative to those shown in Figure 2, single-point energy calculations with better basis sets and effective core potentials would likely redress this.[67] Of greater concern is the identification of stationary points along the two primary reaction pathways, which form the cornerstone of the reaction mechanism. Importantly, structure **6_7aTS** was not found, although all subsequent steps of the pathway leading to **L_2Rh•9** were identified. Likewise, intermediate **18** was not found and, without this intermediate, the decarbonylation pathway, which is important in this system, is less accessible.

(67) Feldgus, S.; Landis, C. R. *J. Am. Chem. Soc.* **2000**, *122*, 12714–12727.

4. Conclusions

The calculated reaction mechanism consisting of two stereochemically distinct pathways is consistent with the observed results for the rhodium-catalyzed hydroacylation of 4-pentenal. Branching of the pathways occurs early in the reaction at the oxidative addition step and the two relevant isomers at this stage are characterized by the position of the acyl group, which, interestingly, is apical in both. Standard trans influence arguments would have predicted the hydride to be apical. Only one of the pathways leads to cyclopentanone product. Low energy side reactions, including isomerization and carbonyl deinsertion, have also been identified and account for the isotopic distribution of products determined experimentally. Importantly, the two pathways can only exchange by returning to the initial complex **6**.

We have also examined the influence of an explicit molecule of solvent or substrate on the reaction energies. Specifically, we have examined its impact on the pathways leading through reductive elimination to product and decarbonylation leading to catalyst death. The experimental trends of solvent dependence and substrate inhibition have been rationalized based on these computational results. Most critically, we have elucidated how high concentrations of substrate facilitate reductive elimination by preferentially lowering this barrier relative to that leading to decarbonylation and catalyst death.

In this particular catalytic system, the application of a popular QM/MM method yielded results significantly different from the all-electron numerical DFT calculations. Most importantly, key intermediates and transition states were not found. While better basis sets and different partitioning schemes within the QM/MM approach will certainly lead to greater success, modeling this rhodium-catalyzed hydroacylation reaction with standard B3LYP/LANL2DZ:UFF QM/MM methods was less able to account for the experimental results.

Acknowledgment. East Carolina University and the National Science Foundation (CHE-0415484 - A.T.M., CNS-0619285 - A.L.S.) supported this work.

Supporting Information Available: Cartesian coordinates and total energies (in hartrees) of all structures presented herein. This material is available free of charge via the Internet at http://pubs.acs.org.

OM700842D